

UNIVERSIDADE ESTADUAL DE CAMPINAS
SISTEMA DE BIBLIOTECAS DA UNICAMP
REPOSITÓRIO DA PRODUÇÃO CIENTÍFICA E INTELLECTUAL DA UNICAMP

Versão do arquivo anexado / Version of attached file:

Versão do Editor / Published Version

Mais informações no site da editora / Further information on publisher's website:

<https://journals.aps.org/prb/abstract/10.1103/PhysRevB.90.235120>

DOI: 10.1103/PhysRevB.90.235120

Direitos autorais / Publisher's copyright statement:

©2014 by American Physical Society. All rights reserved.

DIRETORIA DE TRATAMENTO DA INFORMAÇÃO

Cidade Universitária Zeferino Vaz Barão Geraldo

CEP 13083-970 – Campinas SP

Fone: (19) 3521-6493

<http://www.repositorio.unicamp.br>

Physical properties and magnetic structure of the intermetallic CeCuBi₂ compound

C. Adriano,^{1,*} P. F. S. Rosa,^{1,2} C. B. R. Jesus,¹ J. R. L. Mardegan,^{1,†} T. M. Garitezi,¹ T. Grant,² Z. Fisk,² D. J. Garcia,³
A. P. Reyes,⁴ P. L. Kuhns,⁴ R. R. Urbano,¹ C. Giles,¹ and P. G. Pagliuso¹

¹*Instituto de Física “Gleb Wataghin”, UNICAMP, Campinas-SP, 13083-859, Brazil*

²*University of California, Irvine, California 92697-4574, USA*

³*Instituto Balseiro, Centro Atomico Bariloche, CNEA and CONICET, 8400 Bariloche, Argentina*

⁴*National High Magnetic Field Laboratory, FSU, Tallahassee, Florida 32306-4005, USA*

(Received 7 July 2014; revised manuscript received 25 November 2014; published 10 December 2014)

In this work we combine magnetization, pressure dependent electrical resistivity, heat capacity, ⁶³Cu nuclear magnetic resonance (NMR), and x-ray resonant magnetic scattering experiments to investigate the physical properties of the intermetallic CeCuBi₂ compound. Our single crystals show an antiferromagnetic ordering at $T_N \simeq 16$ K and the magnetic properties indicate that this compound is an Ising antiferromagnet. In particular, the low temperature magnetization data revealed a spin-flop transition at $T = 5$ K when magnetic fields of about 5.5 T are applied along the c axis. Moreover, the x-ray magnetic diffraction data below T_N revealed a commensurate antiferromagnetic structure with propagation wave vector $(00\frac{1}{2})$ with the Ce³⁺ moments oriented along the c axis. Furthermore, our heat capacity, pressure dependent resistivity, and temperature dependent ⁶³Cu NMR data suggest that CeCuBi₂ exhibits a weak heavy fermion behavior with strongly localized Ce³⁺ 4*f* electrons. We thus discuss a scenario in which both the anisotropic magnetic interactions between the Ce³⁺ ions and the tetragonal crystalline electric field effects are taking into account in CeCuBi₂.

DOI: [10.1103/PhysRevB.90.235120](https://doi.org/10.1103/PhysRevB.90.235120)

PACS number(s): 71.20.Lp, 71.27.+a, 75.25.-j, 75.50.Ee

I. INTRODUCTION

A series of rare-earth based intermetallic compounds is usually of great interest to explore the interplay between Ruderman-Kittel-Kasuya-Yoshida (RKKY) magnetic interaction, crystalline electrical field (CEF), and the Fermi surface effects frequently present in these materials. The Ce-based materials can have especially interesting physical properties that arise from the combination of these effects with a strong hybridization between the Ce³⁺ 4*f* and the conduction electrons. Therefore, these materials may present a variety of nontrivial ground states, including unconventional superconductivity (SC) and non-Fermi-liquid behavior frequently exhibited in the vicinity of a magnetically ordered state [1,2]. Interestingly, some of these properties, such as the concomitant observation of unconventional SC and heavy fermion (HF) behavior, seem to be favored in systems with tetragonal structure. Well known examples are the Ce-based heavy fermions superconductors CeMIn₅ ($M = \text{Co, Rh, Ir}$), Ce₂MIn₈ ($M = \text{Co, Rh, Pd}$), CePt₂In₇ ($M = \text{Co, Rh, Ir, Pd}$) [3–7], and CeCu₂Si₂ [8,9].

Recent attention has been given to the CeTX₂ family ($T =$ transition metal, $X =$ pnictogen) and in particular to the CeTSb₂ compounds [10], which host ferromagnetic members with complex magnetic behavior, such as Ce(Ni,Ag)Sb₂. Their physical properties have motivated the investigation of the parent CeTBi₂ compounds [11–13], although studies on the latter are rather rare. Thamizhavel *et al.* [12] have shown that CeCuBi₂ orders antiferromagnetically with a Néel temperature of $T_N = 11.3$ K and an easy axis along the c direction. Nevertheless, no detailed microscopic investigation regarding the relevant magnetic interactions have been presented so far.

It is also intriguing that no HF superconductors have ever been discovered within the CeTX₂ family. Another remarkable result is the breakdown of the De Gennes scaling revealed by non-Kondo members of the REAgBi₂ [14] and RECuBi₂ [15] (RE = rare earth) families. This usually indicates a complex and nontrivial competition between RKKY interactions and tetragonal CEF [16–18].

In this work we report the physical properties and magnetic structure of CeCuBi₂ single crystals. CeCuBi₂ is an intermetallic compound that crystallizes in the tetragonal ZrCuSi₂-type structure ($P4/nmm$ [11] space group and lattice parameters $a = 4.555(4)$ Å and $c = 9.777(8)$ Å) with a stacking arrangement of CeBi-Cu-CeBi-Bi layers. Our results revealed an antiferromagnetic ordering at $T_N = 16$ K, a higher value than reported previously [11,12], suggesting our crystals are of higher quality. In fact, we also found that the Néel temperature is suppressed in Cu-deficient crystals. For example, the compound CeCu_{0.6}Bi₂ orders antiferromagnetically at $T_N = 12$ K. The magnetic structure determination of CeCuBi₂ revealed a propagation vector $(0\ 0\ \frac{1}{2})$ with the magnetic moments aligned along the c axis. A systematic analysis of the magnetization and specific heat data within the framework of a mean field theory with influence of anisotropic first-neighbors interaction and tetragonal CEF [17] allowed us to extract the CEF scheme for CeCuBi₂. It also led us to estimate the values of the anisotropic RKKY exchange parameters between the Ce³⁺ ions. In addition, the analyses of electrical resistivity under hydrostatic pressure and ⁶³Cu nuclear magnetic resonance (NMR) data suggest a scenario where CeCuBi₂ might display a weak heavy fermion behavior with rather strong localized Ce³⁺ 4*f* electrons.

II. EXPERIMENTAL DETAILS

Single crystals of CeCuBi₂ and LaCuBi₂ (a nonmagnetic reference) were grown from Bi flux, as reported previously

*Corresponding author: cadriano@ifi.unicamp.br

†Present address: Deutsches Elektronen-Synchrotron DESY, Hamburg 22603, Germany.

[15]. The crystallographic structure was verified by x-ray powder diffraction and the crystal orientation was determined by the usual Laue method. The system was submitted to elemental analysis using a commercial energy dispersive spectroscopy (EDS) microprobe and a commercial wavelength dispersive spectroscopy (WDS). For oxygen free surface samples the stoichiometry is 1:1:2 with an error of 5%.

Magnetization measurements were performed using a commercial superconducting quantum interference device (SQUID). The specific heat was measured using a commercial small mass calorimeter that employs a quasiadiabatic thermal relaxation technique. The in-plane electrical resistivity was obtained using a low-frequency ac resistance bridge and a four-contact configuration. Electrical-resistivity measurements under hydrostatic pressure were carried out in a clamp-type cell using Fluorinert as a pressure transmitting medium. Pressure was determined by measuring the superconducting critical temperature of a Pb sample.

X-ray resonant magnetic scattering (XRMS) measurements of CeCuBi₂ were carried out at the 4-ID-D beamline at the Advanced Photon Source of the Argonne National Laboratory, IL. The sample was mounted on a cryostat installed in a four-circle diffractometer with the *a* axis parallel to the beam direction. This configuration allowed σ -polarized incident photons in the sample. The measurements were performed using polarization analysis, with a LiF(220) crystal analyzer, appropriate for the energy of Ce *L*₂ absorption edge (6164 eV).

NMR experiments were performed at the National High Magnetic Field Laboratory (NHMFL) in Tallahassee, FL. A CeCuBi₂ single crystal was mounted on a low temperature NMR probe equipped with a goniometer, which allowed a fine alignment of the crystallographic axes with the external magnetic field. A silver wire NMR coil was used in this experiment. The field-swept ⁶³Cu NMR spectra ($I = 3/2$, $\gamma_N/2\pi = 11.285$ MHz/T) were obtained by stepwise summing the Fourier transform of the spin-echo signal.

III. RESULTS AND DISCUSSIONS

Figures 1(a) and 1(b) show the temperature dependence of the magnetic susceptibility $\chi(T)$ when the magnetic field ($H = 1$ kOe) is applied parallel χ_{\parallel} [Fig. 1(a)] and perpendicular χ_{\perp} [Fig. 1(b)] to the crystallographic *c* axis. These data show an antiferromagnetic (AFM) order at $T_N \simeq 16$ K and a low temperature magnetic anisotropy consistent with an easy axis along the *c* direction. The ratio $\chi_{\parallel}/\chi_{\perp} \approx 4.5$ at T_N is mainly determined by the tetragonal CEF splitting and reflects the low-*T* Ce³⁺ single ion anisotropy. The inverse of the polycrystalline $1/\chi_{\text{poly}}(T)$ is presented in Fig. 1(c). A Curie-Weiss fit to this averaged data for $T > 150$ K (dashed line) yields an effective magnetic moment $\mu_{\text{eff}} = 2.5(1) \mu_B$ (in agreement with the theoretical value of $\mu_{\text{eff}} = 2.54 \mu_B$ for Ce³⁺) and a paramagnetic Curie-Weiss temperature $\theta_p = -23(1)$ K.

Figure 1(d) displays the low temperature magnetization as a function of the applied magnetic field $M(H)$. The large magnetic anisotropy of CeCuBi₂ is also evident in these data. We found an abrupt spin-flop transition from an antiferromagnetic to a ferromagnetic (FM) phase at $H \approx 55$ kOe when the magnetic field is applied parallel to the *c* axis (open

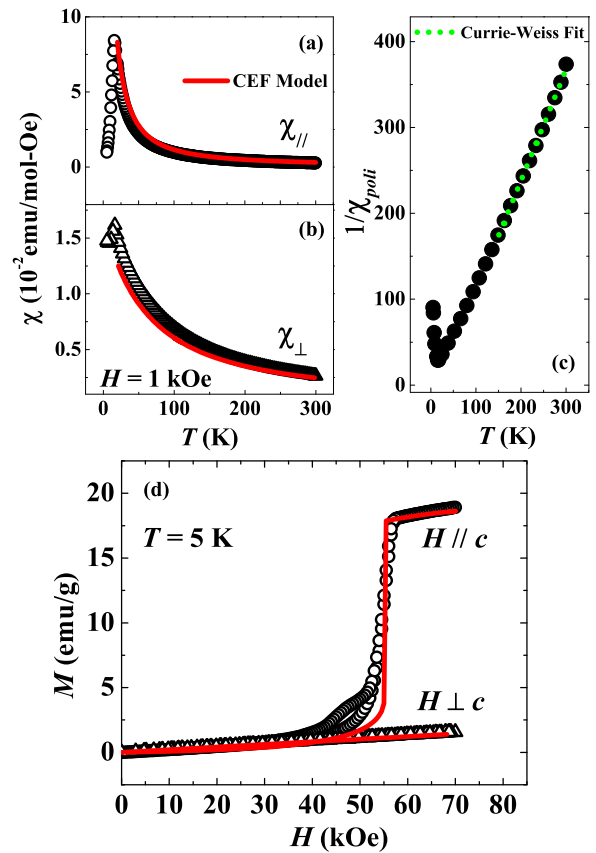


FIG. 1. (Color online) Temperature dependence of the magnetic susceptibility measured with $H = 1$ kOe applied (a) parallel χ_{\parallel} , and (b) perpendicular χ_{\perp} to the *c* axis. (c) Inverse of the polycrystalline average $1/\chi_{\text{poly}}(T)$. The green-dashed line represents a Curie-Weiss fit for $T > 150$ K. (d) Magnetization as a function of the applied magnetic field parallel (open circles) and perpendicular (open triangles) to the *c* axis at $T = 5$ K. The solid lines through the experimental points in (a), (b), and (d) represent the best fits using a CEF mean field model discussed in detail ahead.

circles) while a linear behavior is observed when the field is applied perpendicular to the *c* axis (open triangles) for fields up to $H = 70$ kOe. Interestingly, the $M(H)$ data show a small hysteresis around $H \sim 50$ kOe, suggesting a first-order character for this field induced phase transition. The solid lines through the data points in Figs. 1(a), 1(b), and 1(d) represent the best fits using a CEF mean field model discussed in detail ahead.

The total specific heat divided by the temperature $C(T)/T$ as a function of temperature for CeCuBi₂ (open squares) is shown in Fig. 2(a). The peak of $C(T)/T$ defines $T_N = 16$ K consistently with the AFM transition temperature observed in the magnetization measurements. Figure 2(b) presents the magnetic specific heat $C_{\text{mag}}(T)/T$ of CeCuBi₂ (solid squares) after subtracting the lattice contribution from the nonmagnetic reference LaCuBi₂ compound [solid line in Fig. 2(a)]. The magnetic entropy recovered at T_N obtained by integrating $C_{\text{mag}}(T)/T$ in this temperature range (not shown) was found to be about 80% of $R \ln 2$ ($R \sim 8.3$ J/mol K). This suggests that the magnetic moments of the Ce³⁺ CEF ground state may be slightly compensated due to the Kondo effect. However,

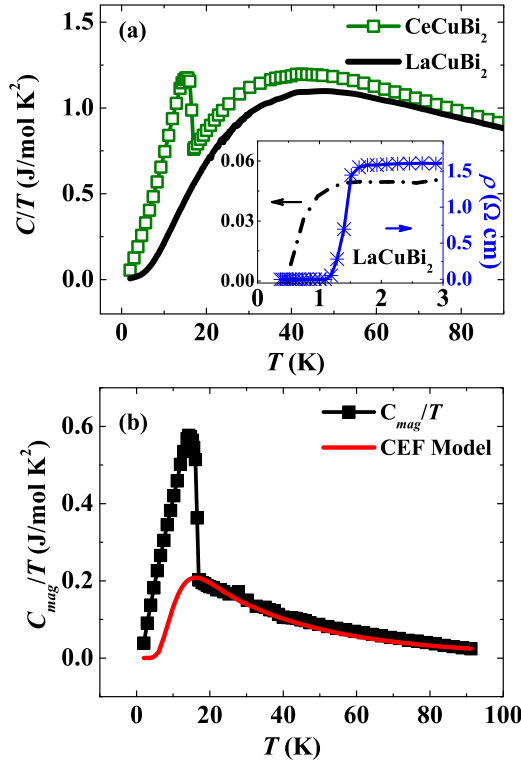


FIG. 2. (Color online) (a) $C(T)/T$ of CeCuBi₂ (open squares) and LaCuBi₂ (solid line) as a function of temperature. The inset shows the SC transition at $T \sim 1.3$ K observed in the low- T specific heat and electrical resistivity data of LaCuBi₂. (b) $C_{\text{mag}}(T)/T$ as a function of temperature. The solid line represents a Schottky-type anomaly resulted from the tetragonal CEF scheme.

the presence of magnetic frustration or simply short range order may also explain the magnetic entropy above T_N . Yet from the $C_{\text{mag}}(T)/T$ data above T_N , it is possible to estimate the Sommerfeld coefficient γ by performing a simple entropy-balance construction [$S(T_N - \epsilon) = S(T_N + \epsilon)$] [19]. Thus, one obtains a $\gamma \sim 50\text{--}150$ mJ/mol K², consistent with the partly compensated magnetic moment of the CEF doublet at the transition.

The inset of Fig. 2(a) highlights the superconducting transition found for LaCuBi₂ at $T \sim 1.3$ K. In fact, conventional superconductivity at similar temperatures has been previously reported for isostructural compounds of the LaMSb₂ family ($M = \text{Ni, Cu, Pd, and Ag}$) [20]. The solid line in Fig. 2(b) represents a Schottky-type anomaly resulting from the tetragonal CEF scheme obtained from our analysis as discussed in the following.

In order to establish a plausible scenario for the magnetic properties of CeCuBi₂, we have analyzed the data presented in Figs. 1 and 2 using a mean field model including the anisotropic interaction from nearest neighbors as well as the tetragonal CEF Hamiltonian. For the complete description of the theoretical model, see Ref. [17]. This model was used to simultaneously fit $\chi(T)$, $M(H)$, and $C_{\text{mag}}(T)/T$ data for $T > 20$ K as a constraint. The best fits yield the CEF parameters: $B_2^0 = -7.67$ K, $B_4^0 = 0.18$ K, and $B_4^4 = 0.11$ K; and two RKKY exchange parameters: $z_{\text{AFM}} * J_{\text{AFM}} = 1.12$ K and $z_{\text{FM}} * J_{\text{FM}} = -1.18$ K, where $z_{\text{AFM}} = 2$ ($z_{\text{FM}} = 4$) is the

Ce³⁺ nearest neighbors with an AFM (FM) coupling, in this case, along the c axis (ab plane). The XRMS experiment suggests a magnetic structure compatible with this scenario, as will be discussed later in this work. It is worth emphasizing that the fits converged only when two distinct J_{RKKY} exchange parameters were considered. Although CeCuBi₂ has an AFM ground state at zero field, the presence of FM fluctuations are evidenced by the presence of a spin-flop transition in the $M(H)$ data. The extracted parameters resulted in a CEF scheme with a $\Gamma_7^{(1)}$ ground state doublet ($0.99|\pm 5/2\rangle - 0.06|\mp 3/2\rangle$), a first excited state $\Gamma_7^{(2)}$ ($0.06|\pm 5/2\rangle + 0.99|\mp 3/2\rangle$) at 50 K, and a second excited doublet Γ_6 ($|\pm 1/2\rangle$) at 149 K.

The obtained CEF scheme and exchange constants account for the main features of the data shown in Figs. 1 and 2, meaning that the magnetic anisotropy, the spin-flop transition, and the Schottky anomaly in $C_{\text{mag}}(T)/T$ are all well explained by this model. However, it is important to notice that the CEF parameters obtained from the fits to macroscopic measurements data may not be as precise and unique. An accurate determination of the CEF scheme and its parameters does require a direct measurement by inelastic neutron scattering [21], while the mixed parameters of the wave functions may be compared with a x-ray absorption study [22]. Nonetheless, apart from a more precise determination of the CEF parameters, the analysis presented here suggests that the Ce³⁺ $4f$ electrons behave as localized magnetic moments. The only indication of a possible Kondo compensation is given by the partially recovered magnetic entropy at T_N ($\sim 80\%$ of $R \ln 2$) and by the rough estimate of γ .

Hence, in order to further investigate the presence of Kondo lattice behavior in CeCuBi₂ we have also performed pressure dependent electrical resistivity. Applied pressure is well known to favor the Kondo effect with respect to the RKKY interaction in Ce-based HF [1–3].

The in-plane electrical resistivity $\rho(T, P)$ of CeCuBi₂ as a function of temperature for several pressures is summarized in Fig. 3. The electrical resistivity at ambient pressure first decreases with decreasing temperature, but it increases back for temperatures below ~ 150 K. Then, $\rho(T, P = 0)$ reaches a maximum at about 50 K and then drops abruptly after the magnetic scattering becomes coherent, as typically found for Ce-based HF [1–3]. At lower temperatures, a small kink is

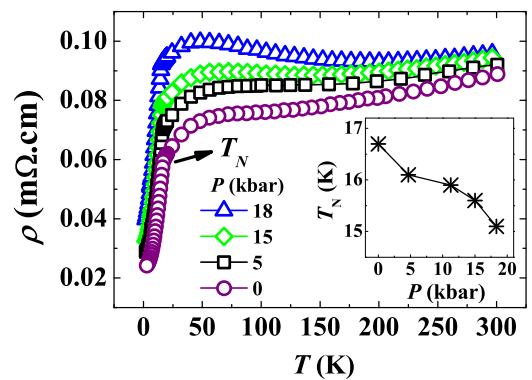


FIG. 3. (Color online) Temperature dependence of the electrical resistivity for different values of applied hydrostatic pressure up to 18 kbar. The inset shows the variation of T_N as a function of pressure.

observed at $T_N = 16$ K. As pressure is increased, a small increase of the room- T resistivity value is observed together with the decrease of T_N . This effect can be seen in the inset of Fig. 3. Such suppression of T_N as a function of pressure is consistent with the increase of the Kondo effect on the $\text{Ce}^{3+} f$ electrons. However, the slope dT_N/dP is relatively small and might be an indication that the $\text{Ce}^{3+} f$ electrons remain rather localized in the studied pressure range.

To gain a more microscopic insight about the magnetic interactions present in CeCuBi_2 , its magnetic structure was investigated by XRMS technique at the $\text{Ce } L_2$ absorption edge in order to enhance the magnetic signal from Ce^{3+} ions below T_N . Magnetic peaks were observed in the dipolar resonant condition at temperatures below ~ 16 K at reciprocal lattice points forbidden for charge scattering and consistent with a commensurate antiferromagnetic structure with propagation vector $(00\frac{1}{2})$.

To determine the possible irreducible magnetic representations Γ^{XRMS} associated with the space group $P4/nmm$, the propagation vector $(00\frac{1}{2})$, and a magnetic moment at the Ce sites, we used the program SARAH [23]. The magnetic representation can be decomposed in terms of four nonzero irreducible representations (IRs Γ_2^{XRMS} , Γ_3^{XRMS} , Γ_9^{XRMS} , and $\Gamma_{10}^{\text{XRMS}}$) written in Kovalev's notation [24]. Within the possible IRs Γ_2^{XRMS} and Γ_3^{XRMS} correspond to a magnetic structure with the Ce magnetic moments pointing along c direction and Γ_9^{XRMS} and $\Gamma_{10}^{\text{XRMS}}$ correspond to Ce magnetic moments lying in the ab plane. Also, Γ_2^{XRMS} and $\Gamma_{10}^{\text{XRMS}}$ correspond to a FM coupling of the Ce ions within the unit cell forming a $(++--)$ sequence (model I), and Γ_3^{XRMS} and Γ_9^{XRMS} correspond to an AFM coupling of the Ce ions within the unit cell forming a $(+-+)$ sequence (model II), both along the c direction.

Figure 4 shows typical results for one selected magnetic peak $(0\ 0\ 5.5)$. Figure 4(a) presents the resonant energy line shape showing a single peak 3 eV below the edge and compatible with a pure dipolar resonance. Figure 4(b) shows the intensity as a function of the angle θ , where a pseudo-Voigt fit shows a full width half maximum of 0.023° . Figure 4(c) presents the temperature dependence of the square root of the integrated intensity, which is proportional to the magnetization of Ce^{3+} ions. A pseudo-Voigt peak shape was used to fit longitudinal θ - 2θ scans in order to obtain the integrated intensities and no hysteresis was observed by cycling the temperature.

The results presented in Fig. 4 are consistent with a dipolar resonant magnetic scattering peak in which the magnetic intensity is found only in the σ - π' channel and disappears above T_N . This confirms the magnetic origin of the $(0\ 0\ 5.5)$ reflection due to the existence of an AFM structure that doubles the chemical unit cell in the c direction. For collinear magnetic structures, the intensity of the x-ray resonant magnetic scattering assumes a simple form for dipolar resonances [25]:

$$I \propto \frac{1}{\mu^* \sin(2\theta)} \left| \sum_n f_n^{E1}(\vec{k}, \hat{\epsilon}, \vec{k}', \hat{\epsilon}', \hat{z}_n) e^{i\vec{Q} \cdot \vec{R}_n} \right|^2, \quad (1)$$

where f_n^{E1} is the dipolar resonant magnetic form factor, μ^* is the absorption correction for asymmetric reflections, 2θ is the scattering angle, $\vec{Q} = \vec{k}' - \vec{k}$ is the wave-vector transfer,

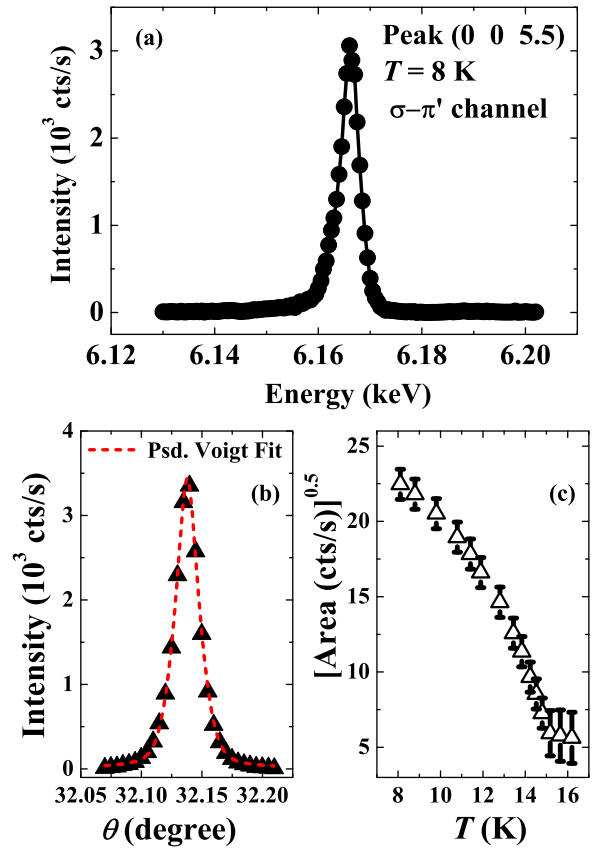


FIG. 4. (Color online) (a) Energy dependence of the XRMS signal of the Ce^{3+} magnetic moment of CeCuBi_2 . (b) Intensity as a function of the angle θ of the crystal through the magnetic peak (005.5) for the σ - π' polarization channel at the $\text{Ce } L_2$ absorption edge. (c) Square root of the intensity as a function of temperature measured with longitudinal (θ - 2θ) from 8 to 16.5 K.

and \vec{k} and \vec{k}' ($\hat{\epsilon}$ and $\hat{\epsilon}'$) are the incident and scattered wave (polarization) vectors, respectively. \vec{R}_n is the position of the n th atom in the lattice, and \hat{z}_n is the moment direction at the n th site. The sum is over the n resonant ions in the magnetic unit cell.

The intensity variation of a magnetic peak as a function of the azimuthal angle can be used to determine the direction of the magnetic moment. In the case of a propagation vector $(0\ 0\ \frac{1}{2})$ the azimuthal dependence of specular magnetic peaks will be constant if the moment is parallel to the c axis and will show a sinusoidal dependence if the moment is perpendicular to the c axis. Figure 5(a) shows the azimuthal dependence of the integrated intensity (σ - π' polarization channel) for two magnetic reflections $(0\ 0\ 3.5)$ and $(0\ 0\ 5.5)$. At each ψ position a θ scan was measured and fitted using a pseudo-Voigt function from which we extracted the integrated intensity value plotted in Fig. 5(a).

As we can see from data in Fig. 5(a), the azimuthal dependence of the integrated intensity of the magnetic peaks have a small variation (within error bars) and presents no sinusoidal periodicity. This result clearly indicates that the moment direction is parallel to the c axis and is in good agreement with the susceptibility measurements of Figs. 1(a)

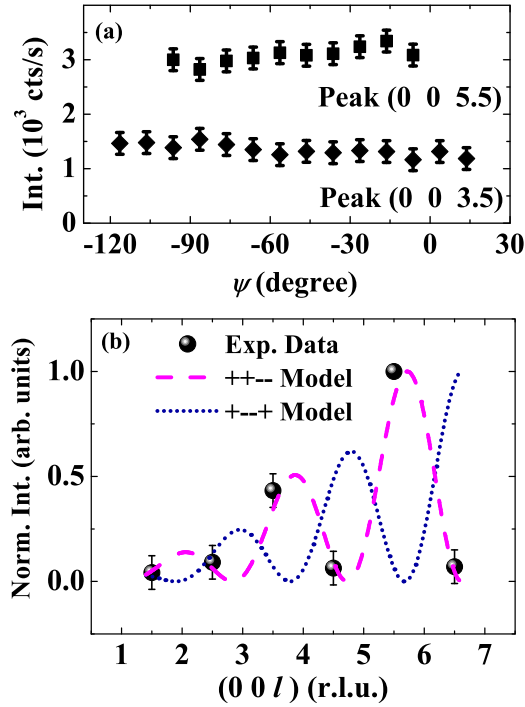


FIG. 5. (Color online) (a) Normalized intensity as a function of the azimuthal angle for (0 0 5.5) and (0 0 3.5) magnetic reflections. (b) Experimental normalized intensity (solid circles) as a function of the l at the reciprocal space direction (0,0, l) at 8 K for σ - π' polarization channel at the Ce L_2 absorption edge. The calculated intensities for two different magnetic couplings are presented as dashed and dotted lines.

and 1(b) that also point to the c axis as the easy magnetization axis.

The magnetic coupling of the Ce atoms within the unit cell can be determined by comparing the experimental integrated intensity of several magnetic peaks with the calculated model [Eq. (1)] [26–28].

Simplifying the absolute square in Eq. (1) for the reflections of the type $(00\frac{l}{2})$, the magnetic intensity is proportional to $\sin^2(\theta + \alpha) * \cos^2(2\pi lz)$ for the model $(++--)$ [or Γ_2^{XRMS}] or $\cos^2(\theta + \alpha) * \cos^2(2\pi lz)$ for the model $(+- -+)$ [or Γ_3^{XRMS}], where z is the position of Ce ions within the unit cell, θ is the Bragg angle, and α is the angle between the vector Q and the c direction. Both magnetic representations consider the magnetic moments aligned parallel to c direction.

Six magnetic peaks of the family $(00\frac{l}{2})$ were measured at $T = 8$ K and compared with the theoretical normalized intensities calculated using the model described by Eq. (1) [Fig. 5(b)]. It is clear that the experimental data follow the $(++--)$ coupling. We can conclude that the correct magnetic structure corresponds to the Γ_2^{XRMS} irreducible representation, i.e., the magnetic moments are aligned parallel to c axis with the $(++--)$ coupling.

Figure 6 represents the magnetic structure of CeCuBi₂ compound where we show two magnetic unit cells (dashed line) for better visualization of the spin coupling along the three directions. One chemical unit cell is represented by the solid line. The heretofore determined magnetic structure of

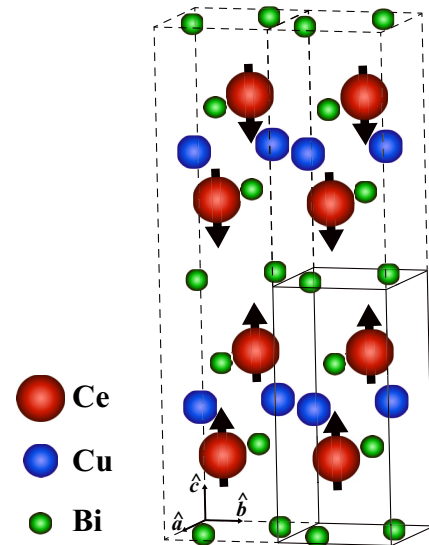


FIG. 6. (Color online) Schematic representation of the magnetic structure of CeCuBi₂. The dashed line defines two magnetic unit cells while the solid line bounds the chemical unit cells.

CeCuBi₂ sheds some light on the global magnetic properties of this compound. The ferromagnetic coupling between the Ce³⁺ moments in the plane is consistent with the presence of FM fluctuations which justifies the need to include two different exchange constants in our mean field model. Indeed, this proposed magnetic structure is compatible with the spin-flop transition to a ferromagnetic phase when a magnetic field is applied along the c axis.

Now, seeking further microscopic information regarding the coupling of the Ce³⁺ $4f$ with the conduction electrons and/or neighboring atoms in CeCuBi₂, we have carried out temperature dependent ⁶³Cu NMR measurements. NMR probes local interactions because it is site specific and sensitive to both electronic charge distribution and magnetic spin.

Figure 7(a) presents a few ⁶³Cu NMR spectra ($I = 3/2$) at temperatures around T_N with the magnetic field applied perpendicular to the c axis. Above $T_N = 16$ K, the ⁶³Cu NMR spectra show a sharp single Lorentzian peak at $H \sim 6.4$ T. We also observed a small peak at around 6.5 T which we associate with one of the ²⁰⁹Bi Zeeman split transitions ($I = 9/2$). Although not the scope of the current investigation, further ongoing experiments will elucidate the origin of this signal. Also, for the low temperature spectra, below T_N , a weak and broad signal is observed at the ⁶³Cu NMR line which might be associated with local field distribution at the ⁶³Cu sites.

The Knight shift $^{63}K_{\perp}$ presented in Fig. 7(b) (left-hand side axis) was obtained from Lorentzian fits of the main peaks shown in Fig. 7(a). The $^{63}K_{\perp}$ is compared with the magnetic susceptibility χ_{\perp} measured with an applied magnetic field of 7 T. These data indicate that the Knight shift tracks the magnetic susceptibility down to $T_N \sim 16$ K. Below this AFM transition, $^{63}K_{\perp}$ is driven by the internal field (hyperfine field) created by the Ce³⁺ $4f$ moments at the Cu sites.

The Ce moments, slightly canted by the external field applied perpendicular to the c axis create a weak ferromagnetic component in the plane responsible for the shift of the resonant

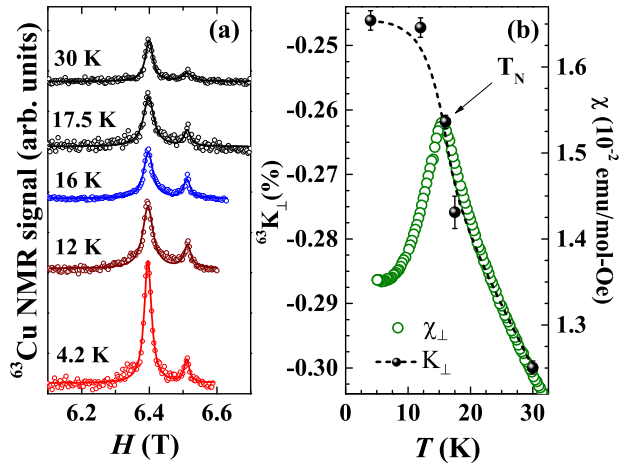


FIG. 7. (Color online) (a) ^{63}Cu NMR spectra ($I = 3/2$) for various temperatures around T_N . (b) The corresponding temperature dependence of the Knight shift (left-hand side scale) compared with the magnetic susceptibility at $H = 7$ T (right-hand side scale). The Knight shift was calculated as $^{63}K_{\perp} = \frac{(\nu/^{63}\gamma_N) - H_r}{H_r}$, with $\nu = 72$ MHz and H_r the peak position of the spectra for each temperature)

peak towards lower fields. Moreover, the relatively small $^{63}K_{\perp}$ found for ^{63}Cu NMR spectra in CeCuBi_2 compared to what is generally found in HF materials [29,30] is consistent with the weak hyperfine coupling constant estimated from the K - χ plot (not shown). This indicates that the Cu 3d electrons are weakly hybridized with the Ce^{3+} 4f local moments [31]. Within this scenario, the dipolar rather than the RKKY interaction seems to be the most relevant mechanism for the weak hyperfine coupling at the Cu sites. Additionally, the sign and strength of the coupling are not strongly influenced by the c -f hybridization as expected in most heavy fermion materials. As such, one may speculate that the strong local moment character of the Ce^{3+} 4f magnetism in CeCuBi_2 is a dominant trend in CeTX_2 family (T = transition metal, X = pnictogen) which makes these families less likely [32] to host HF superconductivity, at least under ambient pressure.

Nevertheless, in a recent work [33], polycrystalline samples of $\text{CeNi}_{0.8}\text{Bi}_2$ have been reported as a heavy fermion superconductor with an AFM transition at ~ 5 K and a SC transition at ~ 4.2 K. The superconducting phase was claimed to be evoked by Ni deficiencies that would presumably create a different ground state than the one realized on single crystalline CeNiBi_2 [12]. The stoichiometric compound was earlier classified as a moderate HF antiferromagnet with $T_N \sim 5$ K, and the presence of a zero resistance transition was associated with contamination of extrinsic Bi thin films. However, a

more recent work has raised important questions about the intrinsic origin of the superconductivity in $\text{CeNi}_{0.8}\text{Bi}_2$. In the report, systematic studies on $\text{CeNi}_{1-x}\text{Bi}_2$ (with $1-x$ varying from 0.64 to 0.85) single crystals [34] revealed that the superconductivity in $\text{CeNi}_{0.8}\text{Bi}_2$ is more likely to be associated with the T_c of the Bi thin films and/or secondary phases of the binaries NiBi and NiBi_3 .

All the above arguments corroborate to our belief that the CeTX_2 compounds do present strong local moment magnetism, with a moderate Kondo compensation implying a weak hybridization between the Ce^{3+} 4f ions and the conduction electrons. In absolute terms, this scenario does not favor a superconducting state.

IV. CONCLUSIONS

In summary, we studied temperature dependent magnetic susceptibility, pressure dependent electrical resistivity, heat capacity, ^{63}Cu nuclear magnetic resonance, and x-ray magnetic scattering on CeCuBi_2 single crystals. Our data revealed that CeCuBi_2 orders antiferromagnetically at $T_N \simeq 16$ K, a value higher than those previously reported for Cu-deficient samples. The detailed analysis of the macroscopic properties of CeCuBi_2 using a mean field model with a tetragonal CEF, enlightened by the microscopic experiments, allowed us to understand the magnetic anisotropy and the realization of a spin-flop first-order-like transition in CeCuBi_2 . These are very compatible with a magnetic field effect on the commensurate antiferromagnetic structure with propagation wave vector $(0\ 0\ \frac{1}{2})$ and Ce moments oriented along the c axis. The combined analyses in this detailed investigation suggest that CeCuBi_2 presents a weak heavy fermion behavior with strongly localized Ce^{3+} 4f electrons subjected to dominant CEF effects and anisotropic RKKY interactions.

ACKNOWLEDGMENTS

This work was funded by São Paulo Research Foundation (Grants No. 2009/09247-3, No. 2009/10264-0, No. 2011/01564-0, No. 2011/23650-5, No. 2011/19924-2, No. 2012/04870-7, No. 2012/05903-6, and No. 2013/20181-0), CNPq, and CAPES-Brazil. The authors thank the 4-ID-D staff of the APS-ANL for the XRMS measurements. R.R.U. is grateful to Dr. Hironori Sakai for enlightening discussions. Work at NHMFL was performed under the auspices of the NSF through the Cooperative Agreement No. DMR-0654118 and the State of Florida. The authors acknowledge the Brazilian Nanotechnology National Laboratory LNNano for providing the equipment and technical support for the EDS experiments.

- [1] A. C. Hewson, *The Kondo Problem to Heavy Fermions* (Cambridge University Press, Cambridge, 1993).
- [2] P. Coleman, C. Pépin, Q. Si, and R. Ramazashvili, *J. Phys. Condens. Matter* **13**, R723 (2001).
- [3] J. D. Thompson and Z. Fisk, *J. Phys. Soc. Jpn.* **81**, 011002 (2012).

- [4] S. Seo, X. Lu, J.-X. Zhu, R. R. Urbano, N. Curro, E. D. Bauer, V. A. Siderov, L. D. Pham, T. Park, Z. Fisk, and J. D. Thompson, *Nat. Phys.* **10**, 120 (2014).
- [5] P. G. Pagliuso, C. Petrovic, R. Movshovich, D. Hall, M. F. Hundley, J. L. Sarrao, J. D. Thompson, and Z. Fisk, *Phys. Rev. B* **64**, 100503(R) (2001).

- [6] N. J. Curro, J. L. Sarrao, J. D. Thompson, P. G. Pagliuso, S. Kos, A. Abanov, and D. Pines, *Phys. Rev. Lett.* **90**, 227202 (2003).
- [7] E. D. Bauer, H. O. Lee, V. A. Sidorov, N. Kurita, K. Gofryk, J. X. Zhu, F. Ronning, R. Movshovich, J. D. Thompson, and T. Park, *Phys. Rev. B* **81**, 180507 (2010).
- [8] F. Steglich, J. Aarts, C. D. Bredl, W. Lieke, D. Meschede, W. Franz, and H. Schäfer, *Phys. Rev. Lett.* **43**, 1892 (1979).
- [9] O. Stockert *et al.*, *Nat. Phys.* **7**, 119 (2011).
- [10] A. Thamizhavel *et al.*, *Phys. Rev. B* **68**, 054427 (2003).
- [11] J. Ye, Y. K. Huang, K. Kadowaki, and T. Matsumoto, *Acta Crystallogr. C* **52**, 1323 (1996).
- [12] A. Thamizhavel *et al.*, *J. Phys. Soc. Jpn.* **72**, 2632 (2003).
- [13] M. H. Jung, A. H. Lacerda, and T. Takabatake, *Phys. Rev. B* **65**, 132405 (2002).
- [14] C. Petrovic, S. L. Bud'ko, J. D. Strand, and P. C. Canfield, *J. Magn. Magn. Mater.* **261**, 210 (2003).
- [15] C. B. R. Jesus, M. M. Piva, P. F. S. Rosa, C. Adriano, and P. G. Pagliuso, *J. Appl. Phys.* **115**, 17E115 (2014).
- [16] P. G. Pagliuso, J. D. Thompson, M. F. Hundley, J. L. Sarrao, and Z. Fisk, *Phys. Rev. B* **63**, 054426 (2001).
- [17] P. G. Pagliuso, D. J. Garcia, E. Miranda, E. Granado, R. Lora Serrano, C. Giles, J. G. S. Duque, R. R. Urbano, C. Rettori, J. D. Thompson, M. F. Hundley, and J. L. Sarrao, *J. Appl. Phys.* **99**, 08P703 (2006).
- [18] R. Lora-Serrano, D. J. Garcia, E. Miranda, C. Adriano, C. Giles, J. G. S. Duque, and P. G. Pagliuso, *Phys. Rev. B* **79**, 024422 (2009).
- [19] H. Hegger, C. Petrovic, E. G. Moshopoulou, M. F. Hundley, J. L. Sarrao, Z. Fisk, and J. D. Thompson, *Phys. Rev. Lett.* **84**, 4986 (2000).
- [20] Y. Muro, N. Takeda, and M. Ishikawa, *J. Alloys Compd.* **257**, 23 (1997).
- [21] A. D. Christianson, E. D. Bauer, J. M. Lawrence, P. S. Riseborough, N. O. Moreno, P. G. Pagliuso, J. L. Sarrao, J. D. Thompson, E. A. Goremychkin, F. R. Trouw, M. P. Hehlen, and R. J. McQueeney, *Phys. Rev. B* **70**, 134505 (2004).
- [22] T. Willers, Z. Hu, N. Hollmann, P. O. Körner, J. Gegner, T. Burnus, H. Fujiwara, A. Tanaka, D. Schmitz, H. H. Hsieh, H.-J. Lin, C. T. Chen, E. D. Bauer, J. L. Sarrao, E. Goremychkin, M. Koza, L. H. Tjeng, and A. Severing, *Phys. Rev. B* **81**, 195114 (2010).
- [23] A. Wills, *Physica B* **276-278**, 680 (2000).
- [24] O. V. Kovalev, *Representations of the Crystallographic Space Groups*, 2nd ed., edited by H. T. Stokes and D. M. Hatch (Gordon and Breach, Yverdon, Switzerland, 1993).
- [25] J. P. Hill and D. F. McMorrow, *Acta Crystallogr. Sect. A* **52**, 236 (1996).
- [26] R. Lora-Serrano, C. Giles, E. Granado, D. J. Garcia, E. Miranda, O. Agüero, L. Mendonça Ferreira, J. G. S. Duque, and P. G. Pagliuso, *Phys. Rev. B* **74**, 214404 (2006).
- [27] C. Adriano, R. Lora-Serrano, C. Giles, F. de Bergevin, J. C. Lang, G. Srajer, C. Mazzoli, L. Paolasini, and P. G. Pagliuso, *Phys. Rev. B* **76**, 104515 (2007).
- [28] C. Adriano, C. Giles, E. M. Bittar, L. N. Coelho, F. de Bergevin, C. Mazzoli, L. Paolasini, W. Ratcliff, R. Bindel, J. W. Lynn, Z. Fisk, and P. G. Pagliuso, *Phys. Rev. B* **81**, 245115 (2010).
- [29] Y.-F. Yang, R. Urbano, N. J. Curro, D. Pines, and E. D. Bauer, *Phys. Rev. Lett.* **103**, 197004 (2009), and references therein.
- [30] T. Ohama, H. Yasuoka, D. Mandrus, Z. Fisk and J. L. Smith, *J. Phys. Soc. Jpn.* **64**, 2628 (1995).
- [31] E. Kim, M. Makivic, and D. L. Cox, *Phys. Rev. Lett.* **75**, 2015 (1995).
- [32] L. Mendonça Ferreira, T. Park, V. Sidorov, M. Nicklas, E. M. Bittar, R. Lora-Serrano, E. N. Hering, S. M. Ramos, M. B. Fontes, E. Baggio-Saitovich, H. Lee, J. L. Sarrao, J. D. Thompson, and P. G. Pagliuso, *Phys. Rev. Lett.* **101**, 017005 (2008).
- [33] H. Mizoguchi, S. Matsuishi, M. Hirano, M. Tachibana, E. Takayama-Muromachi, H. Kawaji, and H. Hosono, *Phys. Rev. Lett.* **106**, 057002 (2011).
- [34] X. Lin, W. E. Straszheim, S. L. Bud'ko, and P. C. Canfield, *J. Alloys Compd.* **554**, 304 (2012).